Dynamics of coalescence of a compound droplet on a liquid pool

Hiranya Deka[1], Gautam Biswas[1]†, Kirti Chandra Sahu[2], Yash Kulkarni[1] and Amaresh Dalal[1]

[1]Department of Mechanical Engineering, Indian Institute of Technology Guwahati, Guwahati 781 039, Assam, India

[2]Department of Chemical Engineering, Indian Institute of Technology Hyderabad, Sangareddy 502 285, Telangana, India

(Received xx; revised xx; accepted xx)

The partial coalescence dynamics of a compound droplet in a liquid pool is numerically investigated. We study the effect of the ratio of the inner to outer radii (R_r) of the compound droplet while maintaining a constant volume equals to that of a 'simple' droplet of radius, R_{eq}. It is observed that for small values of the radius ratio, the coalescence dynamics is similar to that of a 'simple' droplet, but the partial coalescence is suppressed for large values of R_r. Increasing the value of R_r increases the distance migrated by the inner bubble in the downward direction inside the pool away from the free surface. The location of the bubble after coalescence is found to play an important role in the pinch-off process of the satellite droplet. The influence of the governing dimensionless parameters on the coalescence dynamics has also been investigated.

1. Introduction

Coalescence dynamics of a droplet in a liquid pool has been a fascinating subject of research from many century due to its relevance in natural phenomena (Thomson & Newall 1886; Worthington 1908) and industrial applications (Stone *et al.* 2004). The subject caught the attention of many researchers recently due to its complex nature and rich underlying physics (Thoroddsen & Takehara 2000; Morton *et al.* 2000; Chen *et al.* 2006*a*; Ray *et al.* 2015; Zhang *et al.* 2015; Deka *et al.* 2018). Consequently, different regimes from partial/complete coalescence (at low impact velocity) to splashing (at high impact velocity) have been identified. In partial coalescence, a satellite droplet pinches off, which undergoes a cascading process till the satellite droplet is completely merged in the liquid pool.

When a droplet comes in contact with the free-surface of a liquid pool at a low velocity, it floats until the surrounding fluid trapped between the droplet and the free-surface is drained out. After this, the coalescence occurs forming a neck at the contact point of the droplet and the free-surface, which expands rapidly due to high capillary pressure near the contact region. This results in upward moving capillary waves, and thereby forming a liquid column, followed by a necking process near the contact region. The diameter of the neck is reduced with time due to the inward pull of the surface tension and a satellite droplet is detached (Blanchette & Bigioni 2006; Ray *et al.* 2010). The pinch-off process is influenced by the competition between the vertical and horizontal collapse rates of the liquid column. When the vertical collapse is sufficiently delayed by the upward pull exerted by the capillary waves, the horizontal collapse succeeds in merging the neck

† gtm@iitg.ac.in

and producing a satellite droplet. Charles & Mason (1960) reported that the partial coalescence of a droplet is a consequence of an inviscid instability (Rayleigh 1878) of the liquid column that forms after coalescence. Later on, it was revealed that the dynamics of partial coalescence is primarily governed by gravity, viscosity and interfacial tension (Thoroddsen & Takehara (2000); Chen *et al.* (2006*b*)).

Chen *et al.* (2006*b*) delineated gravity, inertio-capillary, viscosity dominated regimes for the coalescence of a droplet in a liquid pool. The coalescence phenomenon is driven by gravity at higher values of the Bond number, given by $Bo = \rho_1 g D^2/\sigma$, wherein D denotes the droplet diameter, g represents the acceleration due to gravity, σ denotes the interfacial tension, and ρ_1 is the density of the droplet. The viscous effect becomes dominant at lower values of Bo. At intermediate values of Bo, the coalescence phenomenon is driven by inertia and capillary forces. The partial coalescence is primarily observed in the inertio-capillary regime. The effect of the physical properties of the fluids on the coalescence process was reviewed by Kavehpour (2015). Yue *et al.* (2006) also investigated the coalescence dynamics of a droplet in Newtonian and viscoelastc fluids. All these previous studies considered 'simple' droplets.

The aim of the present study is to investigate the coalescence dynamics of a compound liquid droplet in a liquid pool of the same liquid. Aston (1972) investigated the dynamics of a gas-filled hollow raindrop in the presence of aerosols. Subsequently, several researchers (Gulyaev *et al.* 2009; Kumar *et al.* 2013; Li *et al.* 2018) have investigated the impact of a compound droplet on solid surfaces due to its importance in painting, coating and printing technologies. The heat transfer characteristics during the impact of a compound droplet on a heated surface have also been investigated (Zheng *et al.* 2017; Li *et al.* 2018). Gao & Feng (2011) numerically investigated the spreading behaviour of a compound drop on a partially wetting solid substrate and compared with the dynamics of a 'simple' drop. They observed various flow regimes depending on the radius ratio of a compound droplet. However, to the best of the authors' knowledge, the partial coalescence dynamics of a compound droplet has not been investigated yet, which is the subject of the present study.

We investigate the effect of radius ratio, R_r (the ratio of the inner radius to the outer radius of the compound drop) while maintaining a constant volume equals to that of a simple droplet of radius, R_{eq}. The influence of fluid properties on the satellite droplet formation has been studied in terms of the governing dimensionless numbers. The mechanism of the coalescence behaviour has also been addressed. We observed that the location of the inner bubble after the coalescence plays an important role in the pinch-off process of the satellite droplet.

The paper is organized as follows. The problem is formulated in Section 2, wherein the governing equations, numerical method and validation of the present solver are discussed in detail. The results are presented in Section 3 and concluding remarks are given in Section 4.

2. Formulation

The coalescence dynamics of a compound liquid droplet in a liquid pool is investigated via axisymmetric numerical simulations using the volume of fluid (VoF) method based finite-volume flow solver, *Gerris* (Popinet 2009). The schematic diagram showing the initial configuration of the droplet is presented in Fig. 1. The droplet and the liquid in the pool are designated by fluid '1', while the surrounding medium is designated by fluid '2'. The dynamic viscosity and density of fluid '1' and fluid '2' are (μ_1, ρ_1) and (μ_2, ρ_2), respectively. The fluids are assumed to be Newtonian and incompressible.

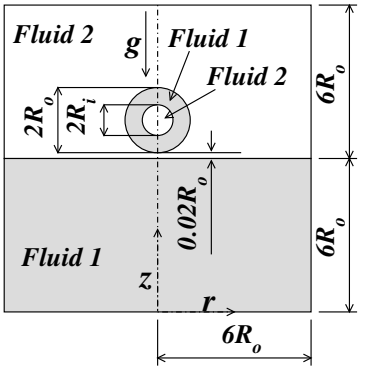

FIGURE 1. Schematic diagram showing the initial configuration of a compound droplet is placed near the free-surface of a liquid pool with zero initial velocity.

A cylindrical coordinate system (r, z) is used to model the flow dynamics, such that $z = 0$ represents the bottom of the computational domain and $r = 0$ is the axis of symmetry. Gravity (g) acts in the negative z direction. The inner and outer radii of the compound droplet are R_i and R_o, respectively. The size of the computational domain is $6R_0 \times 12R_0$, such that the initial height of the liquid pool is $6R_o$. The bottom of the droplet is at $0.02R_o$ from the free surface of the liquid pool. Only half of the domain is considered as axisymmetric simulations are performed in the present study. The computational domain considered in the present study is large enough to have negligible boundary effect.

2.1. *Governing equations*

The continuity and the Navier-Stokes equations govern the flow dynamics, which are given by

$$\nabla \cdot \mathbf{u} = 0, \tag{2.1}$$

$$\rho \left[\frac{\partial \mathbf{u}}{\partial t} + \mathbf{u} \cdot \nabla \mathbf{u} \right] = -\nabla P + \nabla \cdot \left[\mu \left(\nabla \mathbf{u} + \nabla \mathbf{u}^T \right) \right] + \sigma \kappa \hat{n} \delta_s (\mathbf{r} - \mathbf{r}_f) - \rho g \hat{e}_z, \tag{2.2}$$

where $\mathbf{u}(u, v)$ is the velocity field, wherein u and v represent the component of velocity in the radial (r) and vertical (z) directions, respectively; κ is the mean curvature; $\hat{n}$ is the unit normal vector at the interface pointing towards fluid '2'; $\hat{e}_z$ is the unit normal vector in the z direction; $\delta_s(\mathbf{r} - \mathbf{r}_f)$ is a delta distribution function that is zero everywhere except at the interface, where $\mathbf{r} = \mathbf{r}_f$; t denotes time.

The following advection equation for the volume fraction, c of fluid '1', whose value can be taken as 1 and 0 for fluid '1' and fluid '2', respectively, is solved in order to track the interface separating the fluids:

$$\frac{\partial c}{\partial t} + \mathbf{u} \cdot \nabla c = 0. \tag{2.3}$$

The density, ρ and the dynamics viscosity, μ of the fluids are given by

$$\rho = \rho_1 c + \rho_2 (1 - c), \tag{2.4}$$

$$\mu = \mu_1 c + \mu_2 (1 - c). \tag{2.5}$$

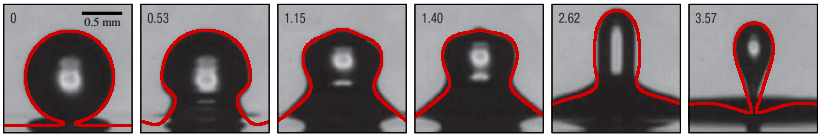

FIGURE 2. Comparison against the experiment of Blanchette & Bigioni (2006) presenting the partial coalescence phenomenon of an ethanol droplet of radius 0.535 mm in air. The present numerical results are shown in red, whereas the background images are the experimental results of Blanchette & Bigioni (2006). The time (in ms) are written on each image. The corresponding dimensionless parameters are $Oh_1 = 1.09 \times 10^{-2}$, $Oh_2 = 2.08 \times 10^{-4}$, $At = 0.997$ and $Bo = 0.09$.

2.2. *Boundary conditions*

The governing equations (Eqs. (2.1) - (2.3)) are solved using the following boundary conditions. The symmetry boundary condition is used at $r = 0$ and the free slip boundary condition is employed at the side boundary ($r = 6R_0$). No-slip and no-penetration boundary conditions are used at the bottom wall ($z = 0$) and the Neumann boundary condition is used at the top of the computational domain ($z = 12R_0$).

2.3. *Non-dimensionalisation*

The governing equations and the boundary conditions are non-dimensionised using the equivalent radius of the compound droplet, $R_{eq}\left(\equiv (R_o^3 - R_i^3)^{1/3}\right)$ as the length scale, $V_s\left(\equiv \sqrt{\sigma/\rho_1 R_{eq}}\right)$ as the velocity scale, and $t_s\left(\equiv \sqrt{\rho_1 R_{eq}^3/\sigma}\right)$ as the time scale, such that

$$(z, r) = R_{eq}(\widetilde{z}, \widetilde{r}),\ (u, v) = V_s(\widetilde{u}, \widetilde{v}),\ \mu = \mu_2(\widetilde{\mu}),\ \rho = \rho_1(\widetilde{\rho}),$$
$$P = \sigma/R_{eq}(\widetilde{P}),\ t = t_s(\widetilde{t}), \tag{2.6}$$

where, tildes designate the dimensionless variables, which are dropped hereafter while presenting the results. The dimensionless numbers used to describe the results are the Bond number, $Bo\left(\equiv \rho_1 g R_{eq}^2/\sigma\right)$, the Ohnesorge numbers associated with fluid '1' and fluid '2', which are given by $Oh_1\left(\equiv \mu_1/\sqrt{\rho_1 \sigma R_{eq}}\right)$ and $Oh_2\left(\equiv \mu_2/\sqrt{\rho_1 \sigma R_{eq}}\right)$, respectively, the Atwood number, $At\,(\equiv (\rho_1 - \rho_2)/(\rho_1 + \rho_2))$, and the radius ratio, $R_r\,(\equiv R_i/R_o)$.

2.4. *Numerical method and validation of the solver*

A VoF method based open source solver, *Gerris* (Popinet 2009) that incorporates a height-function based balanced-force continuum-surface-force formulation for the inclusion of the surface tension term in the Navier-Stokes equations is used. A dynamic adaptive grid refinement is incorporated that provides a large number of grid points/cells in the interfacial region and regions with velocity gradient. The numerical scheme is second order accurate in space and time. Extensive validation exercises of the current numerical methodology have been performed in our previously studies (see for instance, Tripathi *et al.* (2015)). In addition, we have also validated the present solver by comparing with the experimental result of Blanchette & Bigioni (2006) for a 'simple' droplet.

Fig. 2 shows the comparison of the coalescence dynamics of a 'simple' ethanol droplet of radius, $R_{eq} = 0.535$ mm obtained from the present numerical simulation (top row) with the experiment of Blanchette & Bigioni (2006) (bottom row). The corresponding dimensionless numbers are $Oh_1 = 1.09 \times 10^{-2}$, $Oh_2 = 2.08 \times 10^{-4}$, $At = 0.997$ and $Bo = 0.09$. In the experiment of Blanchette & Bigioni (2006), an ethanol droplet was deposited onto the surface of a pool containing ethanol and the dynamics was captured using a high-speed camera. In our computation for this case, initially the droplet with

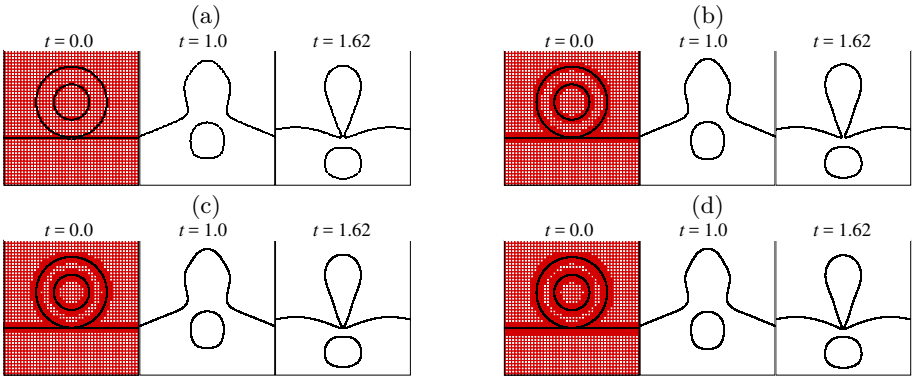

FIGURE 3. Grid convergence test for the coalescence dynamics of an ethanol compound droplet of radius ratio, $R_r = 0.5$: (a) $\Delta = 0.049$ (b) $\Delta = 0.023$, (c) $\Delta = 0.012$ and (d) $\Delta = 0.006$. The rest of the parameters are the same as those used to generate Fig. 2.

zero velocity is placed at a distance $0.02R_{eq}$ over the free-surface of the liquid pool. For $t > 0$, the interstitial air layer drains and the droplet starts to move into the pool (see $t = 0.53$, 1.15 and 1.4 ms). This generates a cylindrical column whose height is higher than that of the initial droplet ($t = 2.62$ ms). The neck of this column narrows down due to the inward pull of the surface tension, and a satellite droplet is pinched off ($t = 3.57$ ms). It can be seen in Fig. 2 that the dynamics obtained from our numerical simulation at different times are in excellent agreement with the experiment of Blanchette & Bigioni (2006). Note that the *Gerris* solver does not use any separate pinch-off criterion, and the pinch-off of satellite droplet is only decided by the smallest cell size. However, it is shown below that after a certain refinement level the results would not change.

A grid convergence test is conducted in Fig. 3 for a compound ethanol droplet of $R_r = 0.5$ coalescing into an ethanol pool. The volume of the compound ethanol droplet is kept the same as that of the 'simple' droplet as considered in Fig. 2. Thus the dimensionless numbers are the same as those used to generate Fig. 2. The simulations are performed using four different meshes using the adaptive mesh refinement feature of *Gerris*. This provides the finest cells in the interfacial region and in the region with velocity magnitude greater than 10^{-2}. The rest of the computational domain are refined based on the velocity magnitude (Popinet 2009). The smallest (dimensionless) cell size, Δ used are 0.049 (Fig. 3(a)), 0.023 (Fig. 3(b)), 0.012 (Fig. 3(c)), and 0.006 (Fig. 3(d)). The corresponding values of R_s/R_{eq}, R_s being the radius of the satellite droplet, are 0.617, 0.61, 0.607 and 0.606. It can also be seen in Fig. 3 that the coalescence dynamics obtained using different meshes are qualitatively similar. The percentage difference between the values of R_s/R_{eq} for $\Delta = 0.012$ and 0.006 is about 0.13 %. Thus, $\Delta = 0.012$ has been used to generate the rest of the results presented in the present study.

3. Results and discussion

We begin the presentation of our results by discussing the mechanism of the coalescence dynamics of a compound droplet in a liquid pool. It is observed that for small radius ratio, R_r, the coalescence dynamics of the compound droplet is similar to that of a 'simple' droplet, where the primary droplet produces a satellite droplet after pinch off. Such a dynamics is presented in Fig. 2. On the other hand, the partial coalescence phenomenon (i.e. the formation of satellite droplet) is not observed in case of a compound droplet with

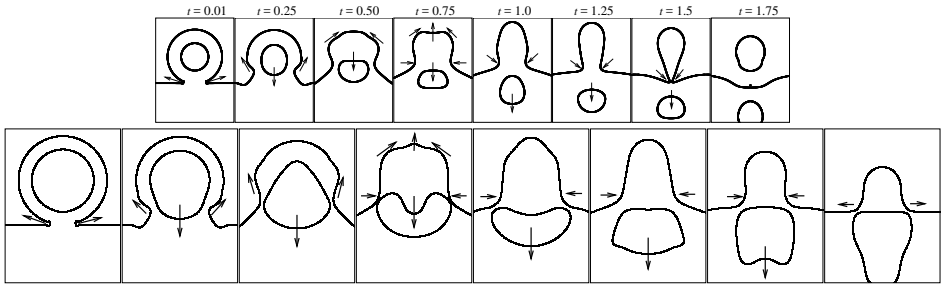

FIGURE 4. The coalescence sequence of a compound ethanol droplet. The radius ratio in the top and bottom row are $R_r = 0.5$ and $R_r = 0.7$, respectively. The rest of the dimensionless numbers are same as those used to generate Fig. 2. Arrow marks indicate the direction of the momentum acting on the interface.

large radius ratio, R_r. The coalescence dynamics of compound droplets with $R_r = 0.5$ and $R_r = 0.7$ are discussed in Fig. 4.

It can be seen in Fig. 4 that at the early stage (as the droplet comes in contact with the free surface), the curvature near the contact region becomes sharp, which in turn generates large capillary pressure near the contact region leading to the rapid expansion of the neck. The uneven curvature of the coalescing droplet creates a pressure difference between the regions above and below the bubble (blob of fluid '2' at the interior of the compound droplet), such that pressure is high above and low below the bubble. As a result, a downward force acts on the bubble and it starts to move in the downward direction, as shown at $t = 0.25$ in Fig. 4. Due to this movement of the bubble in the downward direction, the neck tends to expand in order to create a passage for the bubble, and the resultant capillary waves propagate in the upward direction along the interface of the coalescing droplet as shown by the arrow makes at $t = 0.25$ and 0.5. When these waves reach the top part of the droplet, an upward thrust is generated at the droplet tip as shown at $t = 0.75$. The momentum exerted by the capillary waves delays the vertical collapse of the droplet (forming a column of fluid '1'), while the bubble continues to move in the downward direction due to the pressure difference at the top and bottom portions of the bubble, and the push induces by the drainage of the droplet liquid. The buoyancy opposes the motion of the bubble of fluid '2' (which is lighter than fluid '1'). For the parameter values considered, the abovementioned process is mostly similar till $t = 0.75$ for all values of R_r as shown in the top and bottom rows of Fig. 4. The influence of the propagating capillary waves along the interface was extensively studied by Blanchette & Bigioni (2006); Ding *et al.* (2012); Thoroddsen *et al.* (2007); Ray *et al.* (2010) in case of 'simple' droplets.

In case of a compound droplet with small R_r (i.e. when the inner bubble is small), the pressure difference at the top and bottom portions of the bubble acting in the downward direction dominates the buoyancy force acting in the upward direction. Thus the bubble moves a longer distance in the downward direction as compared to a bigger bubble, i.e. for large R_r. It can be seen in Fig. 4 that for $R_r = 0.5$ (top row) the inner bubble moves far below the neck region of the droplet (see at $t = 1$ and 1.25). Then due to the inward pull of the surface tension, the neck of the column narrows down ($t = 1.5$), and a secondary or satellite droplet is pinched off ($t = 1.75$).

On the other hand, for $R_r = 0.7$, as the size of the inner bubble is big enough, the buoyancy force that acts in the upward direction can not be dominated by the pressure difference acting in the downward direction. Thus the bubble does not move far away from the neck of the fluid '1' column. Another way to compare the dynamics for the

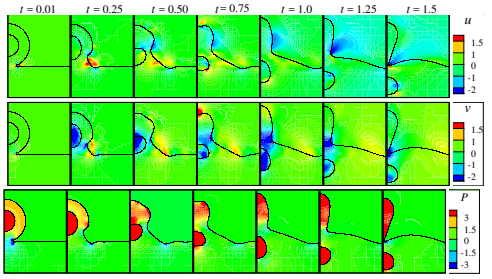

FIGURE 5. The temporal evolution of contours of the radial (u), the vertical (v) components of velocity and the pressure field (P) for a compound droplet with $R_r = 0.5$. The rest of the dimensionless numbers are same as those used to generate Fig. 2.

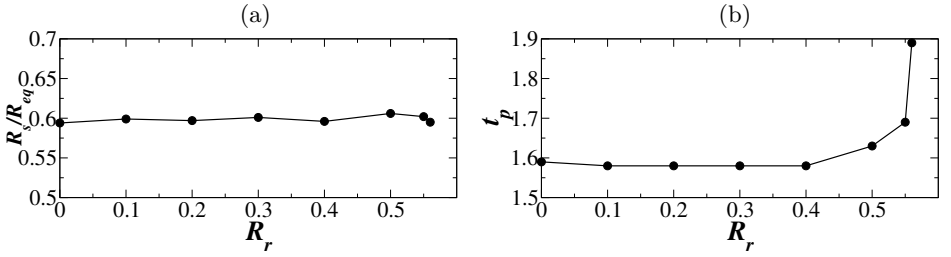

FIGURE 6. The variations of (a) R_s/R_{eq} and (b) t_p versus R_r. The rest of the parameter values are same as those used to generate Fig. 2.

small and large values of R_r is as follows. A big bubble (large R_r) spends more energy to expand the neck in order to make its passage as compared to a small bubble (small R_r). Due to the competition between the buoyancy and the pressure difference acting in the opposite direction, the bubble deforms significantly, which opposes the narrowing of the neck (see the outward arrows on the bubble surface at $t = 1$ and 1.25 in the bottom row of Fig. 4). As a result, the neck does not become thin enough for the pinch-off to occur like in case of $R_r = 0.5$, and finally expands leading to the complete coalescence of the droplet without forming any satellite droplet.

In oder to understand the flow field in the partial coalescence process of a compound droplet, in Fig. 5, we presents the contours of the radial (u) and the vertical (v) components of the velocity, and pressure field (P) for $R_r = 0.5$. It can be seen at the early times ($t \leqslant 0.5$) in the P field (bottom row) that a pressure-difference is created at the top and bottom of the bubble due to the drainage of the droplet into the liquid pool. This pushed the bubble in the downward direction as evident by the development of the negative v velocity at $t \leqslant 0.5$ in the middle row of Fig. 5. During this period, the change in curvature and deformation of the bubble to an oblate shape accompanying by the development of the outward u velocity near the neck and non-zero u velocity contours near the interfacial regions can be seen (top row at $t = 0.5$). As the bubble moves downward, away from the neck region, negative u velocity develops near the neck region as evident at $t \geqslant 1$. The negative radial velocity component becomes sharper at $t = 1.5$ which makes the neck thinner and subsequently leading to the pinch-off of the satellite droplet.

Fig. 6 (a) and (b) present the variations of the ratio between the equivalent radii of the secondary and primary droplets (R_s/R_{eq}) and the pinch-off time, t_p with R_r. Here, R_s represents the equivalent radius of the satellite droplet. The pinch-off time is defined as the time taken from the starting of the coalescence to the pinch-off of the satellite

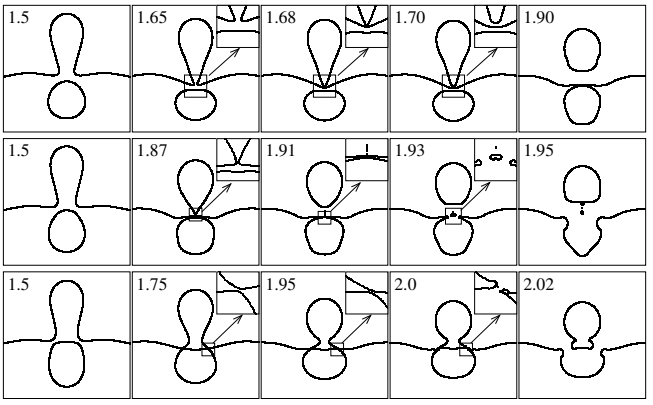

FIGURE 7. Different partial coalescence processes observed for $R_r = 0.55$ (top row), $R_r = 0.56$ (middle row) and $R_r = 0.58$ (bottom row). The rest of the dimensionless numbers are same as those used to generate Fig. 2.

droplet. It can be observed that R_s/R_{eq} remains nearly constant for all the values of R_r considered. The pinch-off time, t_p also remains approximately the same for $R_r \leqslant 0.4$ (see Fig. 6 (b)), which increases sharply for $R_r > 0.4$. For the parameter values considered, we observe that the partial coalescence is completely suppressed for $R_r > 6$ (approximately), which is termed as the critical radius ratio (R_{cr}). The sharp increase in the value of t_p for $0.4 > R_r > 0.6$ can be understood as follows. Near the critical radius ratio, the size of the bubble is enough to create sufficient buoyancy force to oppose its downward motion. This in turn opposes the inward movement of the neck to make it sharper leading to a pinch-off, rather it pushes the interface of the droplet in the outward direction (as also discussed in Fig. 4). This effect is increased at a faster rate with the increase in the value of R_r for $R_r > 0.4$ for this set of parameters. The drainage also slows down due to the presence of the bubble which acts like an obstacle and resists the drainage. As the volume of the compound droplet is kept constant in the present study, although the drainage time of the liquid droplet increases with an increase in the value of R_r, the value of R_s/R_{eq} remains almost constant.

Next, we discuss different types of partial coalescence dynamics observed in case of a compound droplet. We observed three different types of partial coalescence for different values of R_r, namely, (i) pinch off of a satellite droplet without bursting of the bubble, (ii) pinch-off of a satellite droplet before the bursting of the bubble, and (iii) pinch-off of a satellite droplet after bursting of the bubble. These processes are demonstrated in Fig. 7 (a), (b) and (c), which are associated with $R_r = 0.55$, 0.56 and 0.58, respectively. In the last case, it can be seen in Fig. 7 (c) that the detachment of the satellite droplet occurs as a reason of the bubble bursting itself and not because of the pinching of the neck. The different partial coalescence phenomena observed for different values of R_r can be attributed to the decrease in the penetration depth of the bubble with the increase in the the value of R_r, as explained in Fig. 4.

Finally a parametric study is conducted by varying different dimensionless numbers. Fig. 8(a) and (b) presents the variations of R_s/R_{eq} and t_p with the Atwood number, At. Increasing At, i.e. increasing the density contrast between fluid '1' and fluid '2', increases the drainage rate due to the increase in the effective gravitational force, and increases the tendency of the bubble migration in the downward direction. This in turn speeds up the thinning of the neck and decreases the pinch-off time, t_p of the satellite droplet. It can be argued that although increasing At increases the drainage rate, a decrease in the

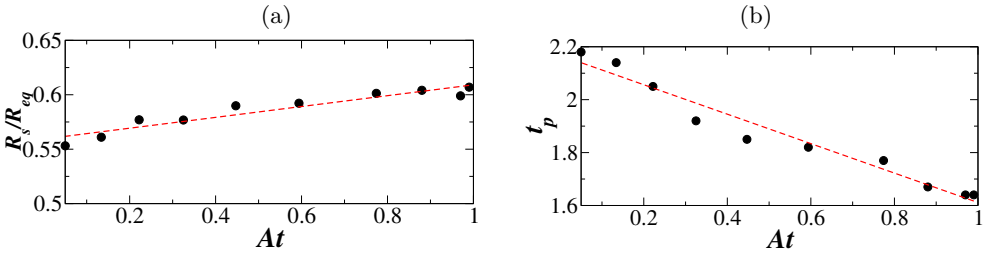

FIGURE 8. The variations of (a) R_s/R_{eq} and (b) t_p with At for $R_r = 0.5$. The rest of the dimensionless numbers are same as those used to generate Fig. 2. The dashed lines in panels (a) and (b) indicate linear fits to the data points.

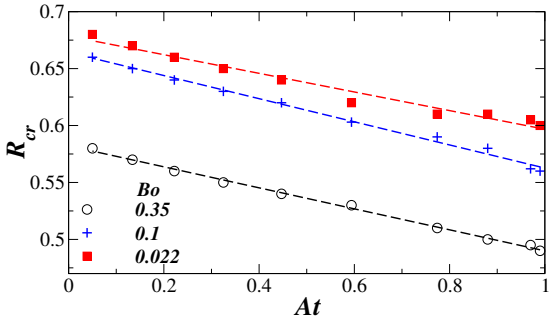

FIGURE 9. The variations of the critical radius ratio, R_{cr} with At for different values of Bo. The dashed lines indicate linear fits to the data points.

pinch-off time decreases the total drainage leading to the decrease in the satellite droplet volume as evident in Fig. 8 (a). Also, increasing At increases the penetration distance of the bubble inside the pool, thereby facilitating the inward movement of the neck resulting in an easer pinch-off. As a result the critical radius ratio, R_{rc} decreases with increasing At, as shown in Fig. 9 for three values of Bo. Inspection of Fig. 9 reveals that for a fixed At, as expected, increasing Bo (decreasing the surface tension over gravitational force) decreases the value of R_{cr}. We observe (not shown) that increasing Oh_1 and Oh_2 has a negligible effect on the critical radius ratio, R_{cr} for the range of parameters considered.

4. Concluding remarks

The partial coalescence dynamics of a compound drop in a liquid pool is investigated via axisymmetric numerical simulations using an open source VoF based flow solver, *Gerris*. The validation of the solver is done by comparing with the experimental result of Blanchette & Bigioni (2006) for a 'simple' drop. The effect of the radius ratio (R_r) of the compound droplet while maintaining a constant volume is studied. We observed that for small R_r, the partial coalescence dynamics is similar to that of a 'simple' drop. However, for the parameters considered, the partial coalescence is suppressed for $R_r > 0.6$ as the inner bubble remains near the free surface and thereby preventing the inward movement of the neck. Three different types of coalescence have been observed for different values of R_r, namely, (i) pinch off of a satellite droplet without bursting of the bubble, (ii) pinch-off of a satellite droplet with the simultaneous bursting of the bubble, and (iii) bubble bursting before the pinch-off. A parametric study is conducted by varying other dimensionless numbers, such as the Atwood and the Bond numbers to identify the critical

radius ratio, R_{cr}, above which partial coalescence is suppressed. The location of the inner bubble in the pool is found to play an important role in the pinch-off process.

REFERENCES

Aston, J. G. 1972 Gas-filled hollow drops in aerosols. *Colloid Interface Sci.* **38**, 547–553.

Blanchette, F. & Bigioni, T. P. 2006 Partial coalescence of drops at liquid interfaces. *Nat. Phys.* **2** (5), 254–257.

Charles, G. E. & Mason, S. G. 1960 The mechanism of partial coalescence of liquid drops at liquid/liquid interfaces. *J. Colloid Sci.* **15** (2), 105–122.

Chen, X., Mandre, S. & Feng, J. J. 2006*a* An experimental study of the coalescence between a drop and an interface in newtonian and polymeric liquids. *Phys. Fluids* **18**, 092103.

Chen, X., Mandre, S. & Feng, J. J. 2006*b* Partial coalescence between a drop and a liquid-liquid interface. *Phys. Fluids* **18** (5), 051705.

Deka, H., Ray, B., Biswas, G. & Dalal, A. 2018 Dynamics of tongue shaped cavity generated during the impact of high-speed microdrops. *Phys. Fluids* **30** (4), 042103.

Ding, H., Li, E. Q., Zhang, F. H., Sui, Y., Spelt, P. D. M. & Thoroddsen, S. T. 2012 Propagation of capillary waves and ejection of small droplets in rapid droplet spreading. *J. Fluid Mech.* **697**, 92–114.

Gao, P. & Feng, J. J. 2011 Spreading and breakup of a compound drop on a partially wetting substrate. *J. Fluid Mech.* **682**, 415–433.

Gulyaev, IP, Solonenko, OP, Gulyaev, P Yu & Smirnov, AV 2009 Hydrodynamic features of the impact of a hollow spherical drop on a flat surface. *Technical Physics Letters* **35** (10), 885–888.

Kavehpour, H. P. 2015 Coalescence of drops. *Ann. Rev. Fluid Mech.* **47**, 245–268.

Kumar, A., Gu, S., Tabbara, H. & Kamnis, S. 2013 Study of impingement of hollow zro2 droplets onto a substrate. *Surf. Coat. Technol.* **220**, 164–169.

Li, D., Duan, X., Zheng, Z. & Liu, Y. 2018 Dynamics and heat transfer of a hollow droplet impact on a wetted solid surface. *Int. J. Heat Mass Transfer* **122**, 1014–1023.

Morton, D., Rudman, M. & Jong-Leng, L. 2000 An investigation of the flow regimes resulting from splashing drops. *Phys. Fluids* **12**, 747–763.

Popinet, S. 2009 An accurate adaptive solver for surface-tension-driven interfacial flows. *J. Comput. Phys.* **228** (16), 5838 – 5866.

Ray, B., Biswas, G. & Sharma, A. 2010 Generation of secondary droplets in coalescence of a drop at a liquid-liquid interface. *J. Fluid Mech.* **655**, 72–104.

Ray, B., Biswas, G. & Sharma, A. 2015 Regimes during liquid drop impact on a liquid pool. *J. Fluid Mech.* **768**, 492–523.

Rayleigh, L. 1878 On the instability of jets. *Proc. Lond. Math. Soc.* **1** (1), 4–13.

Stone, H. A., Stroock, A. D. & Ajdari, A. 2004 Engineering flows in small devices: microfluidics toward a lab-on-a-chip. *Annu. Rev. Fluid Mech.* **36**, 381–411.

Thomson, J. J. & Newall, H. F. 1886 V. on the formation of vortex rings by drops falling into liquids, and some allied phenomena. *Proc. Royal Soc. Lond.* **39** (239-241), 417–436.

Thoroddsen, S. T., Qian, B., Etoh, T. G. & Takehara, K. 2007 The initial coalescence of miscible drops. *Phys. Fluids* **19** (7), 072110.

Thoroddsen, S. T. & Takehara, K. 2000 The coalescence cascade of a drop. *Phys. Fluids* **12**, 1265–1267.

Tripathi, M. K., Sahu, K. C. & Govindarajan, R. 2015 Dynamics of an initially spherical bubble rising in quiescent liquid. *Nat. Commun.* **6**, 6268.

Worthington, A. M. 1908 *A study of splashes*. Longmans, Green, and Co.

Yue, P., Zhou, C. & Feng, J. J. 2006 A computational study of the coalescence between a drop and an interface in newtonian and viscoelastic fluids. *Phys. Fluids* **18** (10), 102102.

Zhang, F. H., Thoraval, M-J, Thoroddsen, S. T. & Taborek, P. 2015 Partial coalescence from bubbles to drops. *J. Fluid Mech.* **782**, 209–239.

Zheng, Z-W, Li, D-S, Qiu, X-Q & Cui, Y-J 2017 Numerical analysis of hollow droplet impact on a flat surface. *Acta Physica Sinica* **66** (1), 14704.